

January 2022

## Heteroaggregation of Lignin-Zein Nanoparticles: Effects of Relative Size and Concentration

Yada Chulakham

Follow this and additional works at: [https://repository.lsu.edu/gradschool\\_theses](https://repository.lsu.edu/gradschool_theses)



Part of the [Other Chemical Engineering Commons](#)

---

### Recommended Citation

Chulakham, Yada, "Heteroaggregation of Lignin-Zein Nanoparticles: Effects of Relative Size and Concentration" (2022). *LSU Master's Theses*. 5486.  
[https://repository.lsu.edu/gradschool\\_theses/5486](https://repository.lsu.edu/gradschool_theses/5486)

This Thesis is brought to you for free and open access by the Graduate School at LSU Scholarly Repository. It has been accepted for inclusion in LSU Master's Theses by an authorized graduate school editor of LSU Scholarly Repository. For more information, please contact [gradetd@lsu.edu](mailto:gradetd@lsu.edu).

# **HETEROAGGREGATION OF LIGNIN AND ZEIN NANOPARTICLES: EFFECTS OF RELATIVE SIZE AND CONCENTRATION**

A Thesis

Submitted to the Graduate Faculty of the  
Louisiana State University and  
Agricultural and Mechanical College  
in partial fulfillment of the  
requirements for the degree of  
Master of Science

in

The Cain Department of Chemical Engineering

by  
Yada Chulakham  
B.S., North Carolina State University, 2017  
May 2022

## **ACKNOWLEDGEMENT**

Foremost, I would like to express my deepest gratitude to my advisor, Dr. Bhuvnesh Bharti, for his expertise and guidance. It is an honor for me to have him as my advisor. This thesis would not have been possible without his contribution. My sincere appreciation goes to my members of committee, Dr. Karsten Thompson and Dr. Mike Benton. I appreciate the time they have taken to read this thesis, as well as their comments and suggestions. I am truly grateful for the opportunity to learn from them both.

I would like to thank my parents. They have always been my greatest support. Their wit and unique vision have helped prepare me for my future. I thank them for their continuous trust in me. I am thankful for my wife. With her full support and care, I am able to overcome the difficulties that occur throughout my studies. Her kindness is heartfelt.

## TABLE OF CONTENTS

ACKNOWLEDGEMENT.....	ii
ABSTRACT.....	iv
CHAPTER 1. INTRODUCTION.....	1
1.1. Nanoparticles and heteroaggregation.....	1
1.2. Environmentally friendly lignin and zein nanoparticles.....	5
CHAPTER 2. EXPERIMENTAL PROCEDURE.....	7
2.1. Materials.....	7
2.2. Synthesis of lignin particles.....	7
2.3. Synthesis of zein particles.....	8
2.4. Aggregate sample preparation.....	10
2.5 Interfacial tension measurement.....	11
CHAPTER 3. RESULTS AND DISCUSSION.....	13
3.1. Herteroaggregation of lignin-zein nanoparticles.....	13
3.2. Herteroaggregation of lignin-zein nanoparticles and oil-water interfacial tension.....	21
CHAPTER 4. CONCLUSION AND FUTURE WORK.....	24
REFERENCES.....	30
VITA.....	34

## **ABSTRACT**

Nanotechnology has become an advanced tool for manufacturing materials of the future. As the size of a material is reduced to a nanoscale, its surface area to volume ratio increases drastically, and its surface property becomes size dependent. This allows scientists to make use of unique properties that nanomaterials have to offer to create novel materials that otherwise could not have been achieved in meter-scale materials. As more industrial companies have planned to incorporate different types of nanomaterials into their products, it is undeniable that some of these nanomaterials will be released to the environment. Such possibility has led to a controversial discussion concerning the impacts of nanoparticles to the environment among the public.

Stable nanoparticles are usually synthesized and stored under a strictly controlled condition. When nanoparticles are released in uncontrollable conditions such as the environment, they are very likely to become destabilized and form aggregates. Heteroaggregates are aggregates that contain two or more nanoparticle species. Synthetic nanoparticles released from manufacturing sites have a high chance of encountering naturally occurring colloids and forming heteroaggregates. However, predicting the fate of heteroaggregation in the environment remains puzzling due to the large variety of possible combinations of different types of nanoparticles.

Most of the nanoparticles currently used in industry are inorganic, which often are hazardous. In recent years, researchers have been trying to utilize biocompatible materials to synthesize green nanoparticles with the hope of creating safer novel nanomaterials. Lignin and zein nanoparticles are environmentally friendly nanomaterials; thus, they serve as ideal alternatives. Nevertheless, a detailed investigation exploring their stabilities and aggregation behaviors must be conducted before integrating them into an industrial-scale production. In this

work, heteroaggregation of lignin and zein nanoparticles is studied. The results indicate that pH, relative size, and concentration of particles of each species directly influence the formation and structure of the heteroaggregates. The effects of heteroaggregation on an oil-water interface is also investigated. Large aggregates are found to produce a stable interface due to the formation of an interfacial film.

# CHAPTER 1: INTRODUCTION

## 1.1. Nanoparticles and Heteroaggregation

The history of nanoparticles can be traced back to the fourth century, when the Romans unintentionally made use of glass containing nanomaterials to create Lycurgas cup (Bayda et al., 2020). The cup appears to have green or red color depending on how light interacts with the cup. Modern scientists analyzed the materials of the cup and found that its glass matrix contained gold and silver nanoparticles in the size range of 50 – 100 nm, which explains the origin of the Lycurgas cup dual color property through light scattering of nanoparticles of different sizes. Now, nanotechnology has progressed to many research areas with promising practical applications in medicine and advanced materials. For example, nanosensors have been developed for detecting specific compounds for medical and biological purposes such as nitric acid in patients with osteoarthritis (Jin et al., 2017) and tetracycline in super drug-resistant pathogens (Jia et al., 2021). Deep understanding in nanoparticle stability from fundamental standpoints is key to successful designs of nanomaterials.

Zeta potential is a common parameter that provides meaningful insights to particle stability (Bhattacharjee, 2016). When a particle suspends in a fluid medium, its surface potential is difficult to evaluate due to the particle's surface interaction with surrounding ions in the fluid environment. To overcome this challenge, zeta potential ( $\zeta$ ) is measured in place of surface potential. Zeta potential measures an electrical potential of a particle at the slipping plane. A slipping plane is the interfacial region where stationary ions and mobile ions coincide. As soon as a particle is introduced to a fluid environment, it attracts surrounding oppositely charged ions to tightly bind to its surface creating a stationary layer of ions called a stern layer. This stern

layer further attracts other positively and negatively charged ions forming a loosely bound layer of ions called a diffuse layer, and next to this layer is where mobile ions in the continuous medium exist. The formation of the stern and diffuse layers creates an electrical double layer, which is the main mechanism that sustains particle stability in an aqueous solvent and keeps the system free of aggregation. Charges located inside the slipping plane travel with the particle as one entity, whereas charges that reside beyond the slipping plane can freely migrate within the medium.

The magnitude of zeta potential can be utilized to predict stability of a dispersed system (Bhattacharjee, 2016). In general,  $-30 \text{ mV} \geq \zeta \geq 30 \text{ mV}$  indicates that the system is dominated by electrostatic repulsive force and, hence, stable. On the contrary, van der Waals attractive force may govern the system when  $-30 \text{ mV} \leq \zeta \leq 30 \text{ mV}$ , which can plausibly lead to the formation of aggregates.

A mathematical model for evaluating colloid stability is famously known as DLVO theory, named after Derjaguin, Landau, Vewery, and Overbeek (Trefalt & Borkovec, 2014). Both electrostatic and van der Waals forces must be considered to obtain a net energy of an interaction between two charged surfaces suspended in an aqueous medium. Electrostatic force mainly governs an interaction at a large separation distance while van der Waals force becomes profoundly crucial as the separation distance decreases. Electrostatic and van der Waals energy curves can be plotted as a function of the separation distance, and a resulted net interparticle interaction energy curve can be constructed.

The net interparticle interaction energy curves consist of primary and secondary minima (Trefalt & Borkovec, 2014). Addition of an electrolyte species can reduce the thickness of an electrical double layer (Debye length). This means that the electrostatic repulsive force is

screened. Once enough electrolyte is added to the system, the Debye length approaches zero, and van der Waals attractive force becomes predominant. This induces the particles to fall into the deep primary minimum; as a result, irreversible aggregates are formed. On the other hand, loose flocculates are trapped in weak secondary minimum at low concentration of electrolyte, which makes the system reversible.

Altering the environment of a dispersed system by varying pH also has a significant impact on aggregation (Bharti et al., 2011). Adsorption of lysosome onto silica nanoparticles can be modified by altering pH. Addition of a basic compound such as sodium hydroxide (NaOH) induces lysosome to adsorb onto the surface of the nanoparticles. Lysosome acts as a bridging agent between silica particles to form heteroaggregates at pH 4-9. Eventually, the presence of HCl or NaOH will neutralize the charge that particles possess. The point at which a particle is neutralized, and zeta potential reaches zero is termed isoelectric (Bhattacharjee, 2016). At neutral point of charge, van der Waals attractive force plays a crucial role in bringing particles to clump together; therefore, aggregation is most likely to occur between a pH range that corresponds to isoelectric points.

Formation of aggregates affects colloidal transport, surface activity, and interaction with surrounding medium. Advanced research in this area provides practical applications to various fields such as diagnosing blood clotting for patients with heart disease (Xin et al., 2021), destabilizing particles for water purification (Lin et al., 2013), and designing demulsifier agents for oil recovery (Elmobarak & Almomani, 2021). In the latter two applications, two or more particle species are often present due to the nature of their contaminants, which leads to the formation of heteroaggregates. However, the study of heteroaggregates is limited because of the

complex variation that arises from particle mixtures that include particle properties, particle to particle interactions, and particle interfacial activities.

Despite endless applications that nanotechnology has to offer, serious health and environmental issues regarding exposure to toxicity have concerned the public due to the highly reactive surface property of nanoparticles (Azimzada et al., 2021). Nanomaterials released to, for instance, a river can encounter biological receptors and cause harm to them. Heteroaggregation is likely to occur because of the large presence of natural minerals and varied pH conditions (Hotze et al., 2010). Moreover, different structures of heteroaggregates may arise due to a wide range of concentration ratios between nanoparticles and other natural particles.

Industry has been mass-producing graphene oxide nanosheets due to their exceptional properties such as high thermal and electrical conductivities; hence, contamination of graphene oxide in the environment is unavoidable. Heteroaggregation of graphene oxide and hematite nanoparticles was studied (Feng et al., 2017). The results showed that their concentration ratio had tremendous effects on rates of aggregation and structures of heteroaggregates. Additionally, many ultrasensitive nanosensors are comprised of gold nanoparticles (Khaliq et al., 2021),(Pothipor et al., 2021),(Zhao et al., 2019); therefore, possibility of gold nanoparticles colliding with natural colloids is inevitable. Smith et al investigated heteroaggregation of gold and hematite nanoparticles (Smith et al., 2015). They found that gold nanoparticles readily attached to hematite nanoparticles under normal conditions of freshwater, and the maximum rate of the heteroaggregation depended on the relative concentration of the two nanoparticles and pH. Thus, understanding parameters that can manipulate heteroaggregation is an effective way to manifest the fate of nanoparticles in the environment.

## 1.2. Environmentally Friendly Lignin and Zein Nanoparticles

Incorporating biocompatible compounds within nanomaterial design has been an active area of research. Lignin is biodegradable since it is plant derived. Silver nanoparticles with lignin-core have been created for antibacterial purposes (Richter et al., 2015). Silver is coated onto lignin-core particles. Once silver ions interact with a targeted cell, they leave lignin-core behind, which can be safely released to the environment. Methods of synthesizing lignin nanoparticles with controlled size and surface functionality has been reported (Richter et al., 2016). Lee et al created a green alternative oil-herding agent by mixing high purity lignin nanoparticles with pentanol (Lee et al., 2018). They believe that there exists a complex interplay between surface tension gradient and lateral capillary attraction created by the lignin particles, which drives particle jamming at the oil-water interface.

Zein is a main protein present in corn and, therefore, biodegradable. Synthesis of zein nanoparticles with controllable size was previously studied (Feng & Lee, 2016). Zein retains a high hydrophobicity, which provides high affinity to oil. A porous material made of zein nanoparticles was also reported as an oil-spill cleanup material (Holley et al., 2021).

Lignin and zein particles are an emerging building block of nanomaterials. Their precursors are readily available in nature, they are nontoxic to humans and environment, and the methods of synthesis can easily be completed. Despite their fruitful potentials, the study of lignin-zein heteroaggregation has never been conducted before. Furthermore, information on how lignin-zein heteroaggregation behaves at oil-water interface is even more limited.

Here, heteroaggregation of lignin-zein nanoparticles will be studied. The origin of the aggregate size will be investigated. The parameters of interest are pH, relative size, and

concentration. The diameter of zein particles will be kept constant at ~130 nm, and the various diameters of lignin particles, which corresponds to the relative sizes of 1.0, 0.8, 0.6, 0.5, and 0.3, will be synthesized. Finally, properties of lignin-zein heteroaggregates at oil-water interface will be explored.

## **CHAPTER 2: EXPERIMENTAL PROCEDURE**

### **2.1 Materials**

High purity lignin (Lignol Innovations Ltd) extracted from organosolv process and acetone (VWR, purity  $\geq 99.5\%$ ) were obtained for synthesis of lignin nanoparticles (NPs). Zein power from corn (Sigma-Aldrich, purity  $\geq 95\%$ ) and ethanol (VWR, purity 99.9%) were utilized to synthesize zein NPs. n-Decane (TCI, purity  $> 99\%$ ), used as the model oil phase in interfacial tension experiments, was obtained from Sigma-Aldrich. HCl and (NaOH) solutions were used to adjust the pH of all sample solutions.

### **2.2 Synthesis of high-purity lignin (HPL) nanoparticles**

Lignin nanoparticles were synthesized according to an antisolvent method as reported by Richter and coauthors (Richter et al., 2016). Lignin completely dissolves in acetone but not in water, and acetone and water are miscible; hence, the two solvents are ideal for this synthesis. Once lignin polymer dissolves in acetone, the lignin-acetone solution can be rapidly added to water. Addition of water induces a flash precipitation of lignin which allows nucleation and growth of nanoparticles to occur. The lignin nanoparticles are brown in appearance. The different sizes of HPL particles can be achieved by using two methods: rate of water addition and an initial amount of lignin in acetone. In this work, varying the initial amount of lignin in acetone is chosen as a method to synthesize different sizes of particles.

Figure 2.1a. illustrates the synthesizing procedure. In short, lignin amount ranging from 0.015 to 0.40 g was dissolved in 10 mL of acetone. The acetone solution was then rapidly poured into 92 mL of deionized (DI) water and allowed to stir for 30 minutes. Undesired large particles were removed by filtering through a 0.45  $\mu\text{m}$  syringe filter. Acetone in the nanoparticle solution

was removed by dialysis in DI water for 24 h. The final diameters of lignin nanoparticles obtained were 45, 60, 80, 105, and 133 nm.

### **2.3 Synthesis of zein nanoparticles**

Zein NPs were synthesized using a previously established method as reported by Feng and Lee (Feng & Lee, 2016). To synthesize zein nanoparticles, 100 mL of 4:1 ethanol:water solvent was mixed with 0.6 g of zein powder. The solution was then rapidly poured into 150 mL of DI water with vigorous stirring. The color of the solution appears creamy, which indicates the formation of zein nanoparticles. Excess ethanol was removed by a rotary evaporator operated at 55°C for 30 minutes. The final removal of remnants of large aggregates was achieved by centrifugation at 4000 rpm for 10 minutes. Zein nanoparticles with a final diameter of 133 nm were acquired. Figure 2.1b. summarizes the procedure.

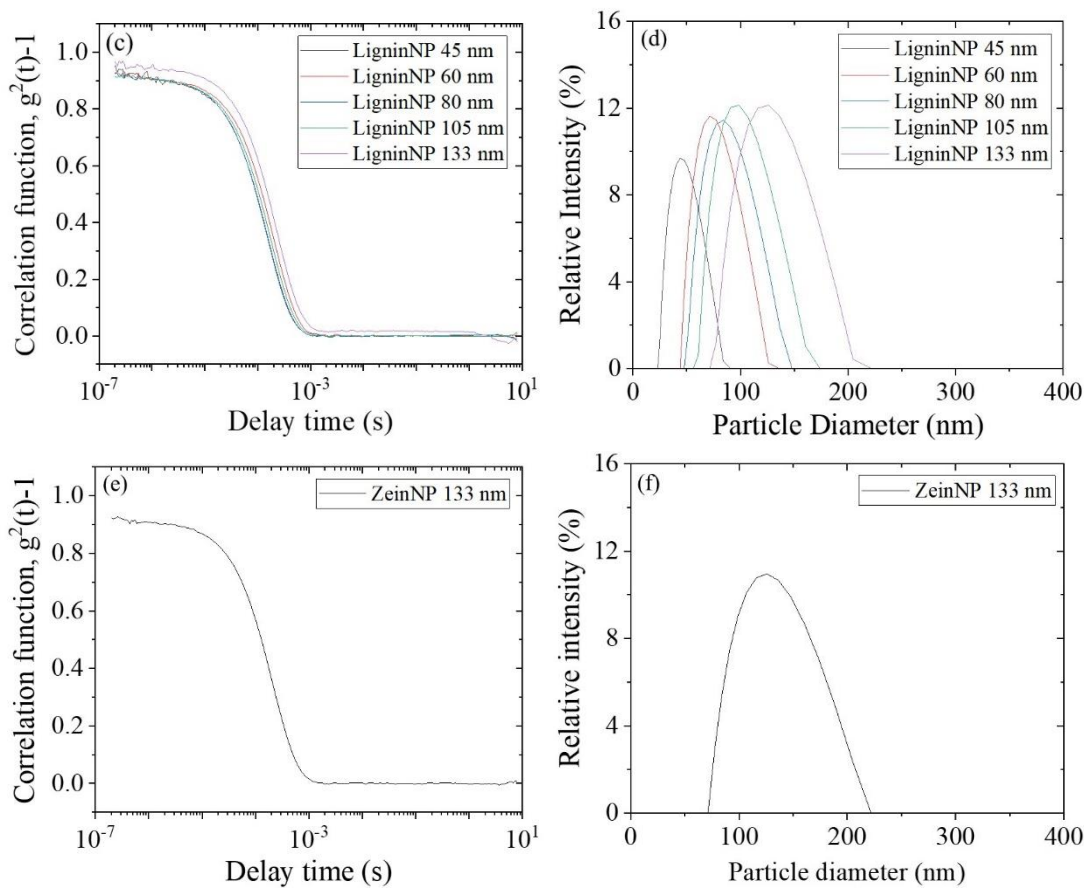
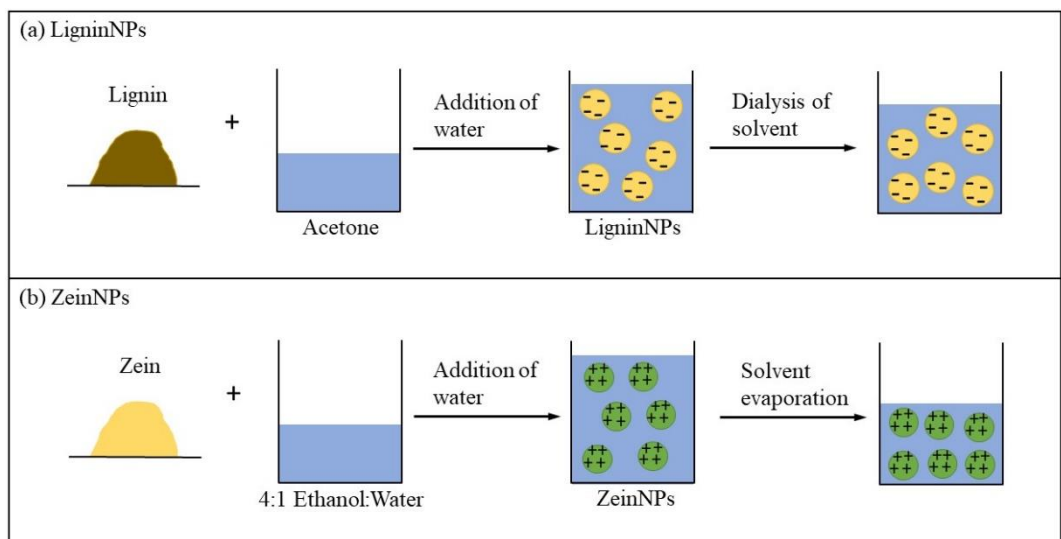


Figure 2.1. Schematics of the syntheses of lignin (a) and zein (b) nanoparticles. Correlation function of lignin (c) and zein (e) nanoparticles. Size distribution of lignin (d) and zein (f) nanoparticles.

## 2.4 Aggregate sample preparation.

Zein nanoparticles of a constant diameter were mixed with five different lignin nanoparticle diameters. The total number of particles maintained constant at  $2.95 \times 10^{12}$ . The pH of samples was adjusted with HCl and NaOH and equilibrated for 24 h at 25°C. The size of particle mixtures was measured using dynamic light scattering (DLS; Brookhaven Instruments) at a 90° angle.

The principle of DLS relies on particle-solvent molecule collision (Goldburg, 1999). Particles suspended in a liquid medium constantly collide with the surrounding solvent molecules enabling the particles to travel freely in any direction within the medium. This random movement of particles is termed Brownian motion. The translational diffusion coefficient ( $D$ ) characterizes the magnitude of Brownian motion defined by the Stokes-Einstein equation (Edward, 1970):

$$D = \frac{k_B T}{6\pi\mu a}$$

where  $k_B$  is Boltzmann's constant,  $T$  is temperature,  $\mu$  signifies viscosity of solvent, and  $a$  represents particle's radius.  $D$  and  $a$  are inversely proportional to each other; therefore, the smaller the particle's radius, the larger the diffusion coefficient, and the faster the particle can diffuse.

DLS is typically equipped with a laser beam, a photon detector, and a correlator (Goldburg, 1999). Once the laser beam interacts with particles in a dispersed system, it scatters off the surface of the particles. The intensity of light scattered is collected by the detector set at a specific angle. Because particles in a dispersed system are constantly moving due to the presence of Brownian motion, the intensity of light fluctuates over time. The correlator then uses the

information of the time-dependent intensity fluctuation to generate the corresponding diffusion coefficient, and the size of the particles can be calculated by evaluating the Stokes-Einstein equation.

## **2.5 Interfacial tension (IFT) measurement.**

A pendant drop of 20  $\mu\text{L}$  nanoparticle solution was created in a 1 cm x 1 cm x 4.5 cm cuvette filled with decane. The adsorption of nanoparticles was monitored by an optical tensiometer (Biolin Scientific) equipped with a high-speed camera, which recorded a time-dependent reduction of IFT as particle mixtures adsorbed at the oil-water interface. Decane is used as a model oil phase.

IFT ( $\gamma$ ) can be measured by evaluating the shape of a pendant drop from the following equation (Berry et al., 2015):

$$\beta = \frac{\Delta\rho g R_o^2}{\gamma}$$

where  $\beta$  is a shape-dependent bond number,  $\Delta\rho$  is density difference, and  $R_o$  is droplet dimension. Figure 2.2 displays a schematic of a pendant drop with all parameters included.

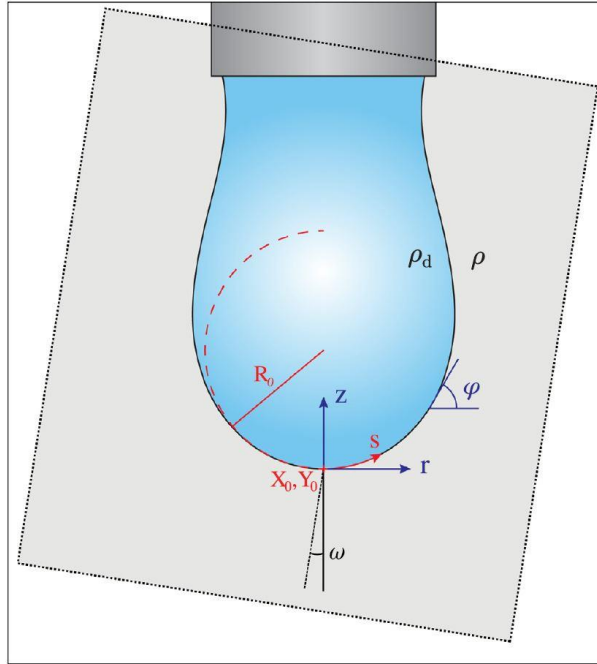


Figure 2.2 Schematic of a pendant drop (Berry et al., 2015).

$\beta$  can be found by solving the Young-Laplace equation expressed in three dimensionless differential equations (Berry et al., 2015):

$$\frac{d\varphi}{ds} = 2 + \beta z - \frac{\sin\varphi}{r}$$

$$\frac{dr}{ds} = \cos\varphi$$

$$\frac{dz}{ds} = \sin\varphi$$

## CHAPTER 3: RESULTS AND DISCUSSION

### 3.1 Heteroaggregation of lignin-zein nanoparticles

Parameters associated with the formation of heteroaggregation of lignin-zein particle are investigated by conducting three sets of experiments. The first set of experiments focuses on establishing the relationship between pH and particle stability. The second set of experiments explores the effects of lignin particles of various sizes on heteroaggregation. The third set of experiments examines the effects of particle concentration on the structures of heteroaggregates. Graphical results are displayed, and the interpretation of the results is elaborated in this chapter.

#### 3.1.1 Effects of pH

To investigate particle stability in relation to pH, samples containing zein and lignin particles were prepared, and their pH was adjusted accordingly by the addition of HCl and NaOH. For simplicity, parameters termed relative size of nanoparticles,  $R$ , ( $R = \frac{\text{Diameter of lignin particles}}{\text{Diameter of zein particles}}$ ) and relative number of particles,  $n$ , ( $n = \frac{\text{Number of lignin particles}}{\text{Number of zein particles}}$ ) are used to describe the system. In this experiment, the diameters of zein and lignin particles were fixed at 130 nm, which corresponded to  $R=1$ . All samples also contained equal number of lignin and zein particles, which could be represented by  $n=1$ . Next, the resulted size of particle mixtures was monitored by DLS. The size of particle mixtures obtained was ~140 nm at the pH range of 5.9 to 10. This indicated that no aggregate was formed within this pH range. The same phenomenon was observed when both species were at pH 2 and lower. On the contrary, the size of particle mixtures increased significantly at a pH range equivalent to pH 2.1 to 5.9. This signified the formation of heteroaggregates. The graph of aggregate size plotted as a function of pH in Figure 3.1b summarizes these behaviors.

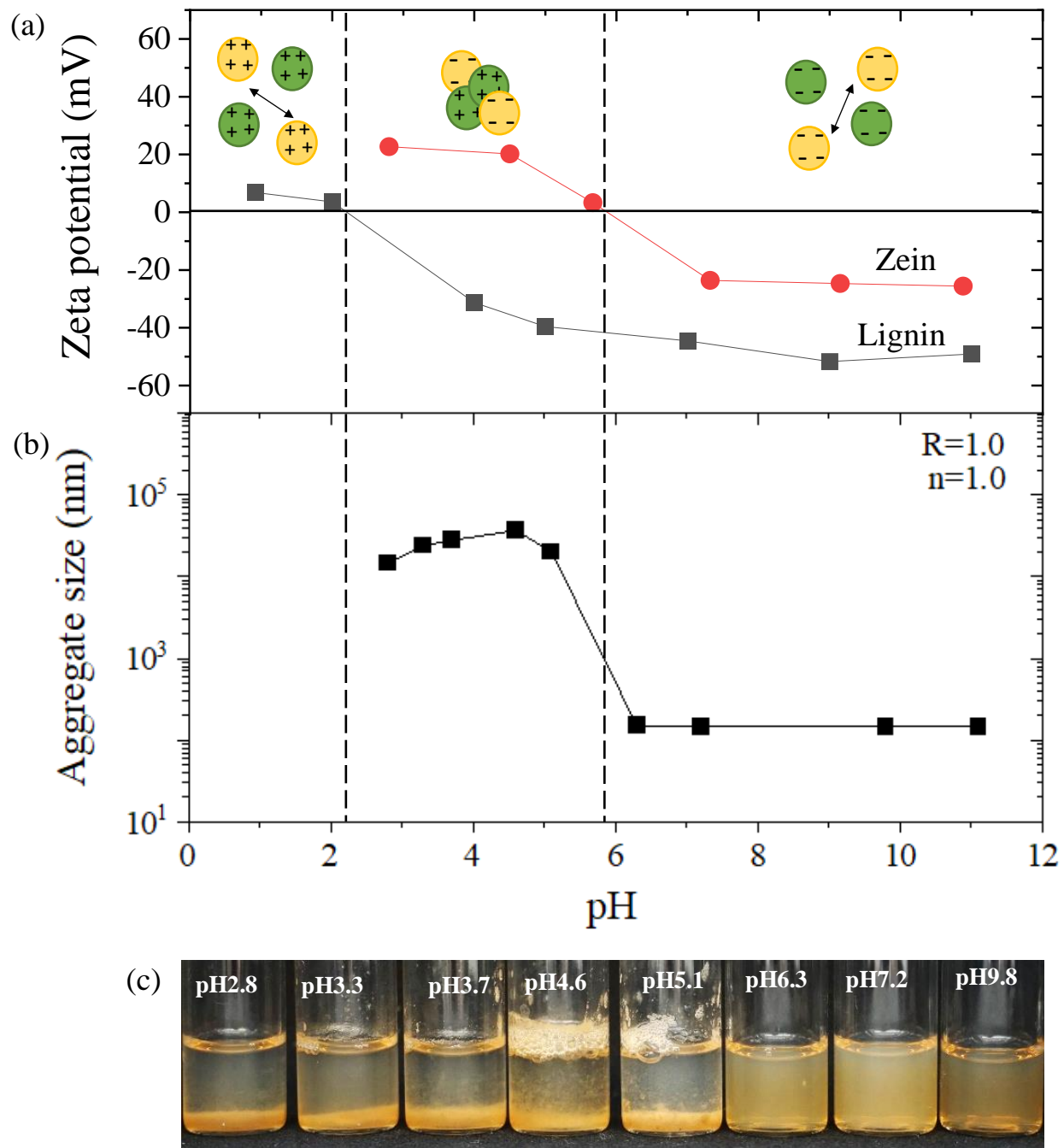


Figure 3.1 Effects of pH on the formation of heteroaggregates. (a) The change in zeta potential of pure lignin and zein nanoparticles is plotted as a function of pH. (b) The change in aggregate size is also shown as a function of pH. (c) The picture of actual sample vials is included for observation.

To determine the origin of aggregate size with respect to pH, zeta potentials of pure lignin and zein nanoparticles were measured as a function of pH by using DLS. The results are displayed in Figure 3.1, where the change of zeta potential is plotted as a function of pH. The isoelectric point of lignin particles was at pH 2.1. At  $\text{pH} < 2.1$ , lignin particles were weakly positively charged, whereas, at  $\text{pH} > 2.1$ , they were strongly negatively charged. Zein particles remained negatively charged at high pH until they reached the isoelectric point at pH 5.9 then became positively charged at  $\text{pH} < 5.9$ .

The evolution of charge fluctuation can be attributed to the dissociation of acid and base. Once HCl dissociated in water, a positive hydrogen ion was created, and this positive ion adsorbed onto the surface of the particles making the particles more positively charged. A similar process occurred when a basic compound was present with particles suspended in water. NaOH dissociated in water and generated a negative hydroxide ion; as a result, the hydroxide ion adsorbed onto the surface of the particles which made the particles more negatively charged.

pH ranges of 0 to 2 and 5.9 to 10 were free of aggregates because the primary interaction in these regions was electrostatic repulsion between lignin and zein particles. When charges of the two components were both negative or both positive, the particles repelled each other; therefore, they were able to maintain their stability. Large heteroaggregates were formed when pH fell within the isoelectric points, because the predominate interaction was electrostatic attraction since lignin and zein particles carried opposite charges.

In summary, the charges of lignin and zein particles suspended in an aqueous medium change upon the addition of an acidic or a basic compound. pH is a major parameter that dictates the occurrence of heteroaggregates. The electrostatic attraction is the main governing force that

causes heteroaggregation to arise at a pH range that resulted in oppositely charged particles. Conversely, the stability of the particles exists between the pH range that results in similarly charged particles because the electrostatic repulsion force repels the particles and prevents them from clumping. pH has a tremendous effect on surface charge and stability of particles. Moreover, by understanding the effect of pH on particle stability, one can utilize this knowledge to systematically control the aggregate size.

### **3.1.2 Effects of relative size of particles**

The next parameter of interest is the relative size of lignin to zein particles. In this part of the experiment, the size of zein particles was fixed at ~130 nm, and R was varied to 0.3, 0.5, 0.6, 0.8, and 1.0. This R corresponded to the sizes of lignin particles 45, 60, 80, 105, and 130 nm, respectively. n was fixed at 1.0. pH of all samples was maintained constant at 4.6 since the maximum difference in zeta potential occurred at this pH. Large aggregates were formed in all R as shown in Figure 3.2a, and Figure 3.2b shows the corresponding correlation function obtained from DLS. The picture of the actual vials is provided in Figure 3.2c. According to Figure 3.2c, the color of the aggregates turns to a creamy color as R decreases. The creamy color signifies the presence of zein nanoparticles as previously mentioned in Chapter 2.3.

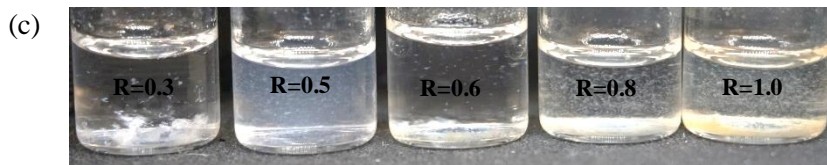
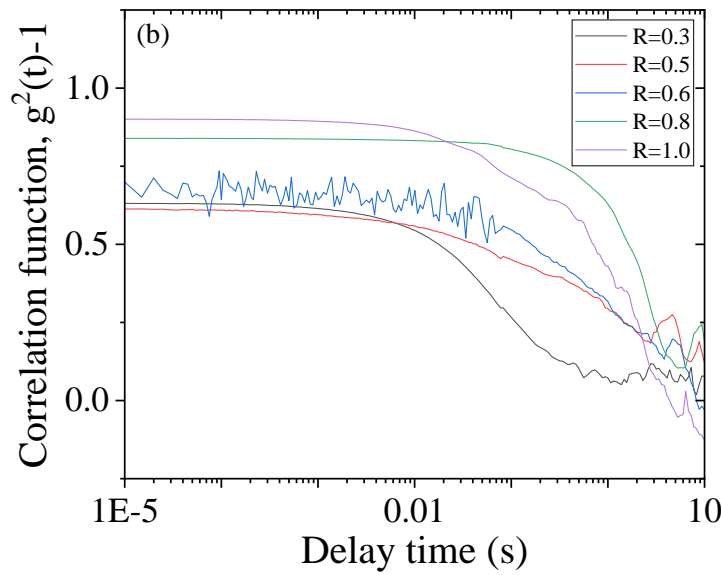
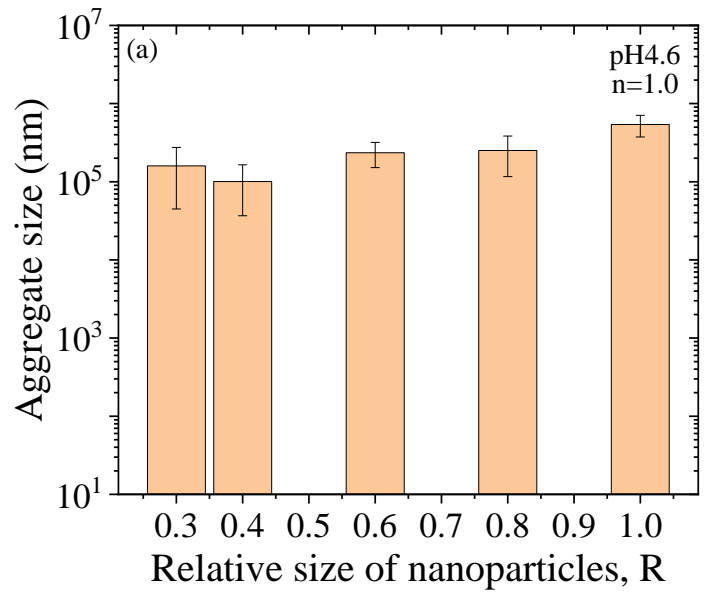


Figure 3.2. The change of aggregate size in relation to R at pH 4.6 and n=1 (a). Correlation function obtained by DLS at different R (b). The picture of aggregates of all R at n=1 (c).

Lignin and zein particles are oppositely charged at pH 4.6; hence, the predominant force between the two species is always electrostatic attraction regardless of different sizes of lignin particles. At  $R = 1$ , a negatively charged lignin particle attaches to another positively charged zein particle, and this dimer further attracts other lignin and zein particles together as the aggregate size is growing. In this case, coprecipitation of lignin and zein particles occur by means of electrostatic attraction. Additionally, the colors of aggregates at  $R=1$  are both creamy and brown, which further indicate the formation of large zein and lignin aggregate structures as displayed in Figure 3.2c.

At  $R < 1$ , smaller lignin particles are also electrostatically attracted to zein particles. The aggregates enlarge as lignin particles act as an electrostatic bridging agent between zein particles. According to Figure 3.2c, the only color of the aggregates formed at  $R=0.3, 0.4, 0.6,$  and  $0.8$  is creamy, which confirms that they mainly consist of large clusters of zein particles.

The contribution from van der Waals attraction is negligible since the particles do not interact at a short-range distance. The separation distance between lignin particles equals to the diameter of a zein particle, and the separation distance between zein particles equals to the diameter of a lignin particle. These distances are large enough to suppress the van der Waals attractive force from having any major effects on aggregation.

### **3.1.3 Effects of relative concentration of particles**

The last parameter of interest is the relative concentration of particles,  $n$ . The experiment begins by varying  $n$  at  $R=1$ . The pH is fixed at 4.6. At  $n=0.1$ , an immediate increase in aggregate size is observed, and the maximum aggregate size occurs at  $n=1$ . As the number of lignin

particles increases, the aggregate size gradually decreases. The results are shown in Figure 3.3a.

Figure 3.3b depicts the appearance of the aggregates formed.

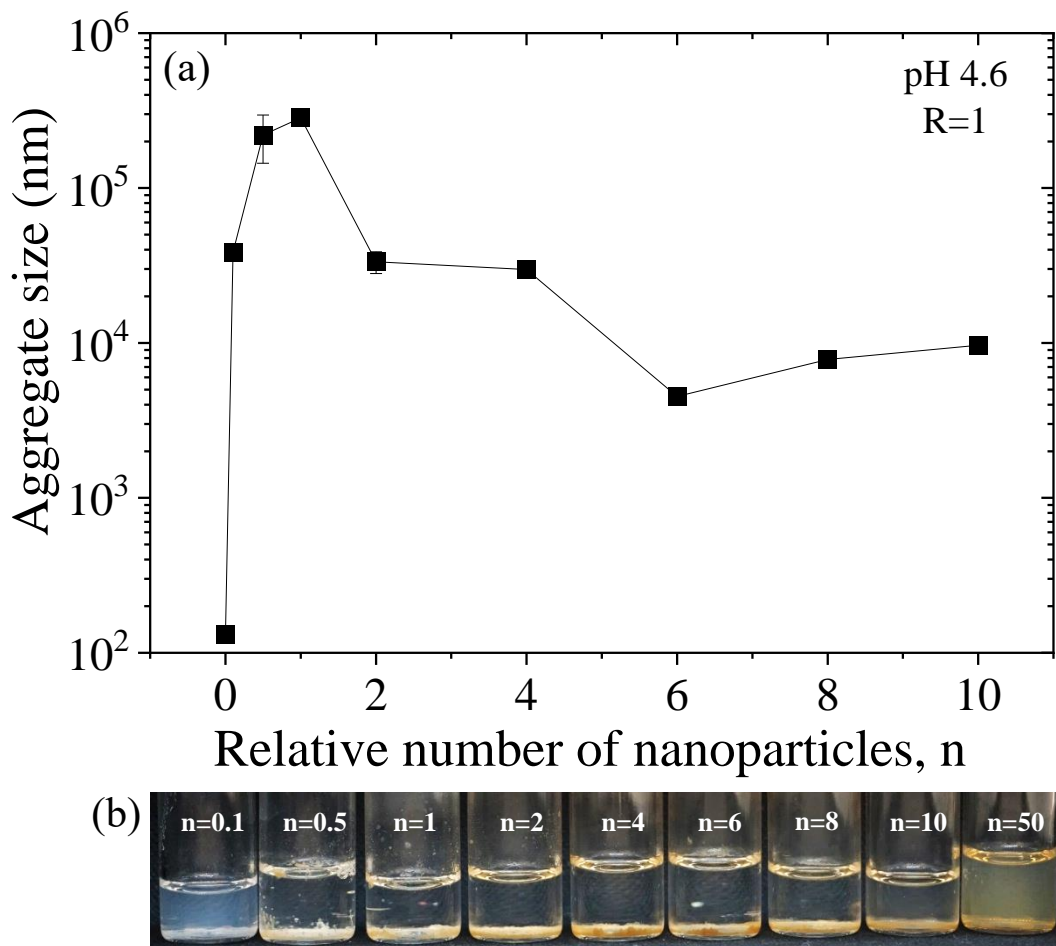


Figure 3.3 Effects of relative number of nanoparticles on heteroaggregates at  $R=1$ . (a) The change of aggregate size is plotted as a function of  $n$ . The maximum size of aggregates occurs at  $n=1$ . The picture of the actual sample vials displays the formation of the aggregates.

According to Figure 3.3b, a turbid color in the bulk solution is observed only when  $n=0.1$ , which indicates that stable zein particles are present in the bulk solution. This can be explained by the fact that lignin particles are unable to neutralize and act as a bridging agent to all zein particles since the number of lignin particles is 10 times less than the number of zein

particles. The color of the aggregates formed is also turbid, which confirms that the majority of the aggregates contain zein particles.

As  $n$  increases, the color of the aggregates appears to be more brown as expected because more lignin particles are electrostatically attracted to the surface of the zein particles. From  $n=0.1$  to  $n=8$ , flocs of aggregates continue to appear until  $n=10$ . At  $n=10$ , the appearance of aggregates changes to fine powder like solids indicating the presence of a smaller structure of aggregates. The presence of the smaller structure suggests that the system is more stable as more lignin particles are introduced. This is further confirmed as  $n$  increases to 50, where no sedimentation of solid is observed.

The effects of relative concentration of lignin to zein particles are also investigated at different  $R$ . Figure 3.4 illustrates the results obtained from DLS. The aggregate size reaches maximum at  $n=1$  and decreases as more lignin particles are added to the system at all  $R$ . At high  $n$  ratio, it is more likely that a zein particle finds itself surrounded by other lignin particles rather than other zein particles simply because of the larger presence of lignin particles in the solution. Furthermore, it is assumed that, once a zein particle encounters a large number of lignin particles, the surface of the zein particle is covered with lignin particles. The adsorption of negatively charged lignin particles makes the entire structure negatively charged. This zein core-lignin shell structure is stable against further aggregation. Similar findings have been reported in literature. Spruijt et al studied oppositely charged polystyrene particles and found that, at a 1:20 particle ratio, a core-shell structure was formed (Spruijt et al., 2011).

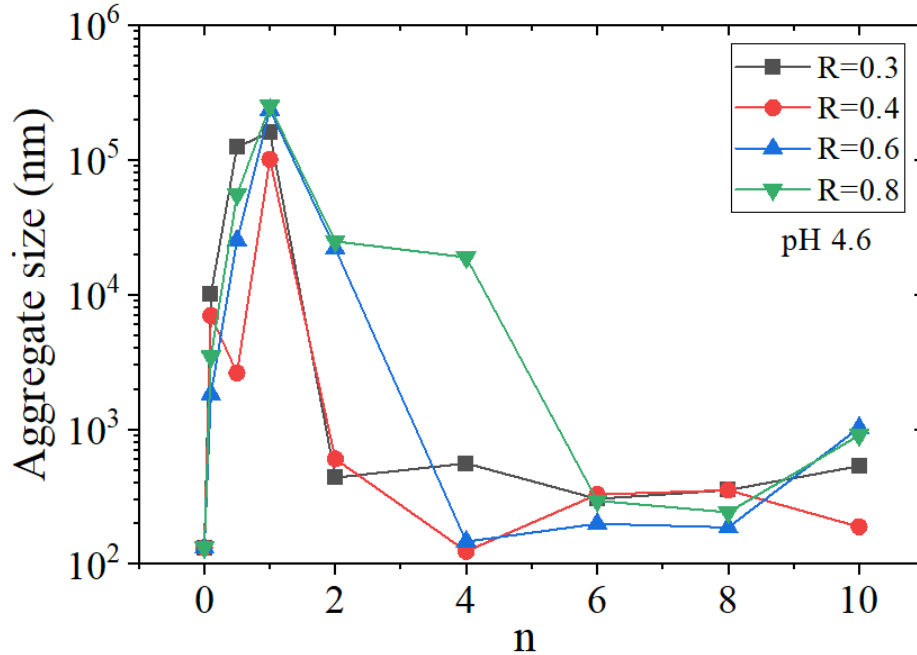


Figure 3.4 The change of aggregate size as a function of  $n$  at different  $R$  values. The largest aggregate size is observed at  $n=1$ .

### 3.2 Heteroaggregation of lignin-zein nanoparticles and oil-water interfacial tension

#### 3.2.1 Effects of heteroaggregation on oil-water interface

Effects of the heteroaggregates on the property of oil-water interface are investigated by conducting an IFT study. Three different samples of  $n=0.1$ , 6, and 10 at  $R=0.4$  were selected. A pendant drop of each sample was submerged in decane. The change in IFT was recorded by a tensiometer equipped with a high-speed camera. The IFT of decane-pure water is 52 mN/m (Zeppieri et al., 2001). The reduction in IFT as a function of time is obtained in all three samples due to the adsorption of aggregates onto the interface. The result is shown in Figure 3.5a.

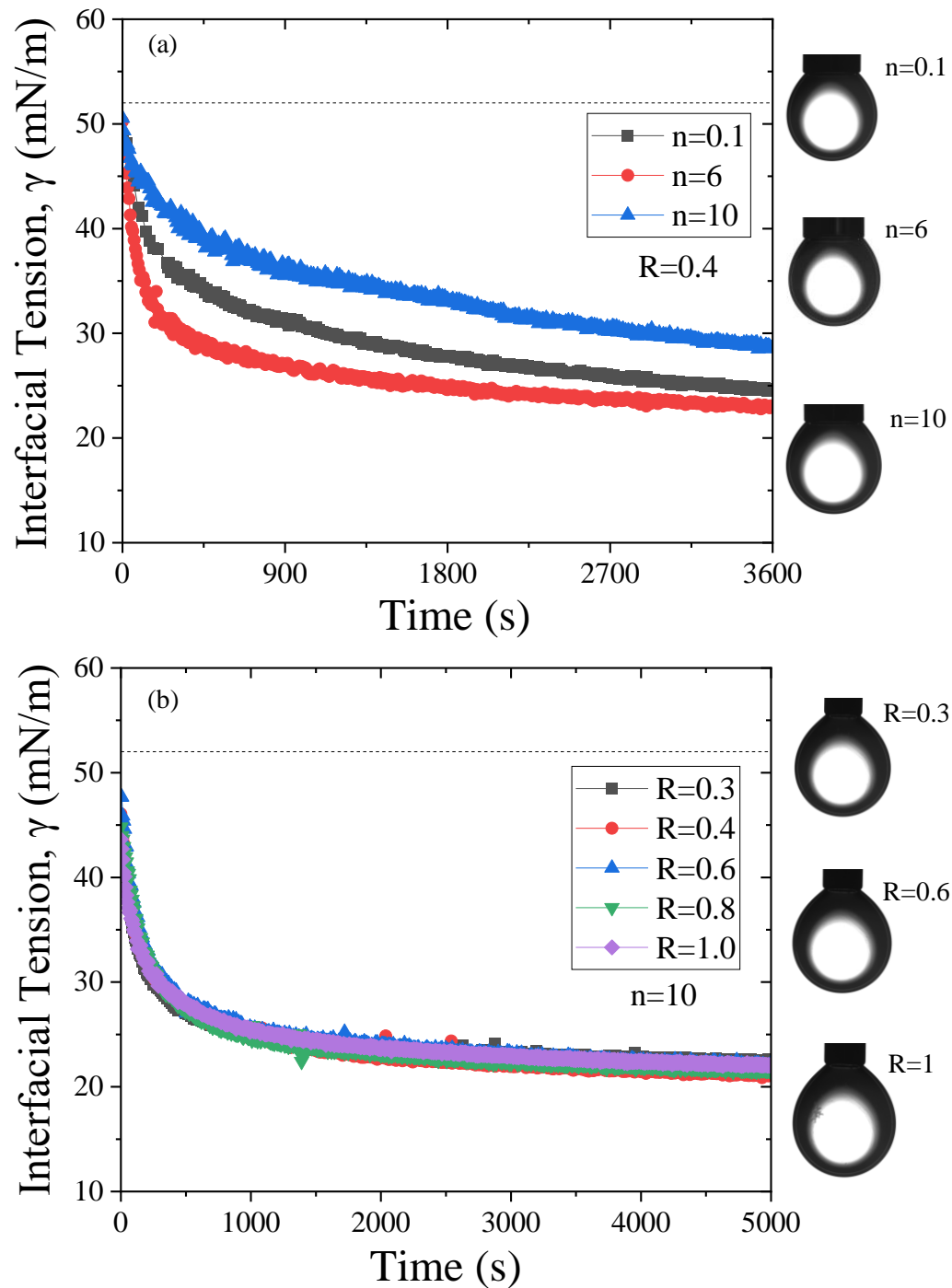


Figure 3.5 The change of interfacial tension as a function of time. Interfacial tension of decane-water containing aggregates for  $R=0.4$  is investigated at three different  $n$  (a). The lowest interfacial tension observed occurs at  $n=6.0$ . Interfacial tensions of all  $n$  are measured at  $n=10$  (b). All samples equilibrate within 5000 seconds. The interfacial tension is independent of  $R$ . The dashed line indicates the IFT of decane-pure water.

The reduction in IFT caused by the adsorption of nanoparticles has been previously reported (Ravera et al., 2006). As soon as the pendant drop is created in the oil phase, the nanoparticles diffuse to the interface due to the presence of nanoparticle concentration gradient between the interface and the bulk. When a particle adsorbs onto the interface, the area at the interface is displaced by the particle, which in turn reduces the contact area between oil and water. As a result, the IFT and free energy at the interface ( $\Delta E$ ) decrease (Hua et al., 2018). The change of free energy associated with particle adsorption can be expressed by this equation (Hua et al., 2018):

$$\Delta E = -\pi r_{NP}^2 \gamma_{OW} (1 \pm \cos \theta_{ow})^2$$

where  $r_{NP}$ ,  $\gamma_{OW}$ , and  $\theta_{ow}$  represent radius of the particle, IFT of oil-water, and particle-fluid contact angle, respectively. Only particles that are partially hydrophobic can adsorb at the interface (Zhang et al., 2017). Since the two particles of interest are partially hydrophobic, they are able to adsorb at the interface. Therefore, it can be inferred that the reduction of IFT observed in the mixture of lignin-zein nanoparticles is caused by the adsorption of the heteroaggregates onto the oil-water interface.

Particle size plays an essential role in determining the free energy of adsorption onto the interface.  $\Delta E$  is directly proportional to  $r_{NP}^2$ . The energy of attachment increases two orders of magnitude as the size of each nanoparticle increases. This energy can reach to several  $k_B T$ , which makes the adsorption of nanoparticles onto the interface irreversible (Binks, 2002). Because of this reason, nanoparticles serve as a better oil-water interfacial stabilizer than molecular surfactants that are much smaller in size. In this work, the size of aggregates is much larger than particles; therefore,  $\Delta E$  of aggregates is anticipated to be significantly higher than  $\Delta E$

of particles. This allows the aggregates to potentially provide a unique stability feature to the interface.

To test the effects of aggregates containing different relative sizes of the particles on the interface, IFT of all five R was measured at  $n=10$ . The IFT of all samples reaches equilibrium at 20 mN/m as shown in Figure 3.5b. The reduction of IFT signifies the adsorption of aggregates. The similar equilibrium IFT of all samples may be attributed to an error in sample preparation such as an excessively high concentration of aggregates in the samples, which saturates the adsorption sites at the interface. Further experimentation should be conducted at a low concentration of aggregates to confirm this behavior. Nevertheless, the free energy of aggregate adsorption of each sample is expected to be different since it contains aggregates of different sizes. This gives rise to various stages of interfacial stability, which can be characterized by performing an interfacial dilational rheology experiment.

### **3.2.2 Effects of heteroaggregation on interfacial dilational rheology**

Interfacial dilational rheology experiments were performed on a tensiometer equipped with a pulsating drop module. In this module, a drop of an aqueous solution is created in a cuvette filled with decane, and an automatic liquid dispenser oscillates the volume of a droplet at a specific frequency.

When the liquid dispenser increases the volume of a droplet, the area of the droplet surface is expanded, the contact area between oil and water at the interface is increased, and, thereby, the interfacial tension is increased. On the other hand, when the volume of a droplet is decreased, the area of the droplet surface is compressed, the contact area between oil and water at the interface is reduced, and the interfacial tension is decreased. The degree of droplet stability

is quantified by dilational viscoelasticity ( $\epsilon$ ).  $\epsilon$  can be defined by the following equation (Ravera et al., 2010):

$$\epsilon = \frac{\Delta\gamma}{\Delta A/A_o} \exp(i\Phi)$$

where  $\Delta\gamma$  is the amplitude of IFT,  $\Delta A$  is the amplitude of the oscillating area,  $A_o$  is the initial area of a droplet, and  $\Phi$  represents the phase shift between the IFT and area. In general, the higher the  $\epsilon$ , the more stable the system. Figure 3.6 depicts all parameters required to evaluate  $\epsilon$ , which can be empirically obtained from the tensiometer.

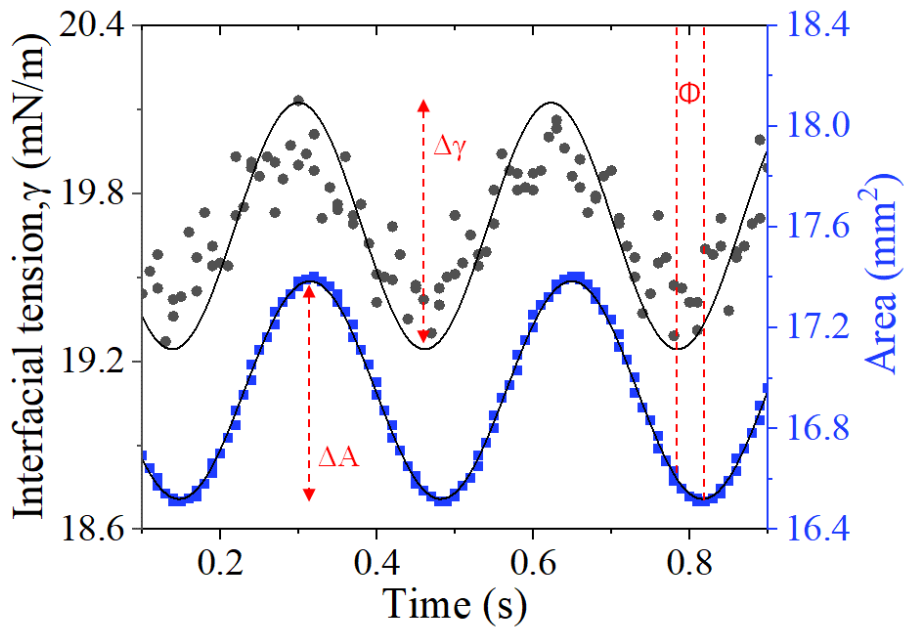


Figure 3.6 A typical response of a droplet oscillatory for analyzing interfacial dilational rheology.

The volume of a droplet corresponding to  $R=1.0$  in Figure 3.5b was oscillated at several frequencies ranging from 0.01-10 Hz. The resulting  $\epsilon$  is plotted as a function of frequency as illustrated in Figure 3.7. The change in  $\epsilon$  at different frequencies is related to the mechanical property of the film created by the adsorption of aggregates.  $\epsilon$  remained approximately constant

at low frequency, which suggests that the film created by aggregates behaves as a rigid body rather than elastic at this frequency. As the frequency increases to 8 Hz,  $\epsilon$  increases dramatically, which indicates that the film expresses a highly elastic behavior. Thus, an adsorption layer behaves uniquely in response to different frequencies.

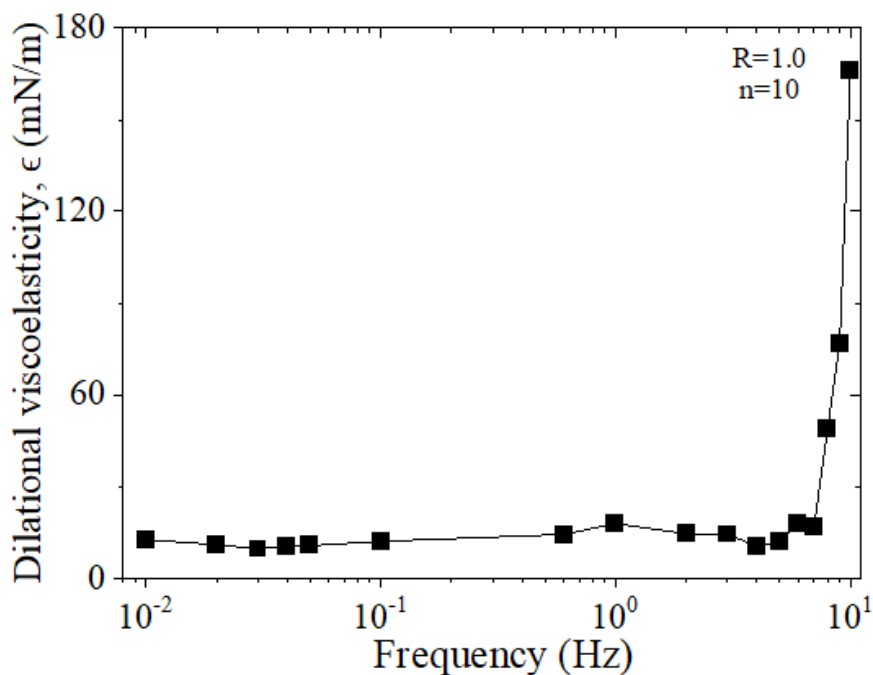


Figure 3.7 The change in dilational viscoelasticity as a function of frequency at  $R=1$  and  $n=10$ . A sharp increase in  $\epsilon$  is observed at high frequencies.

Film formation created by the adsorption of nanoparticles at the oil-water interface has been previously reported (Lee et al., 2018), (Whitby et al., 2012). According to Whitby et al., an increase in  $\epsilon$  was observed at a low frequency range (0.01-0.1 Hz). They also found that higher values of  $\epsilon$  were obtained in a system with silica particles mixed with octadecylamine surfactants as opposed to a system containing octadecylamine surfactants alone due to the irreversible adsorption of the particles driven by their large free energy of attachment ( $\Delta E$ ) (Whitby et al.,

2012). Therefore, a significantly high  $\epsilon$  found in this work can possibly be attributed to an even larger  $\Delta E$  caused by the adsorption of macrostructures of aggregates.

To investigate the viscoelasticity of aggregates containing different relative sizes of the particles on interfacial dilational rheology, the volume of samples corresponded to  $R=0.3, 0.4, 0.6,$  and  $0.8$  in Figure 3.5a were oscillated at 10 Hz since the preliminary result in Figure 3.7 showed that the aggregate film responded the strongest at this frequency. Figure 3.8 shows the change in  $\epsilon$  increases as  $R$  increases. The aggregates of  $R=0.4$  is smaller than the aggregates of  $R=0.3$  as depicted in Figure 3.4, which explains why  $\epsilon$  of  $R=0.4$  is lower than  $\epsilon$  of  $R=0.3$ . Therefore, it can be concluded that a larger size of aggregates produces a more elastic film. It remains to be seen how such elasticity would impact the emulsion formed by the decane-water mixture containing the lignin-zein heteroaggregates.

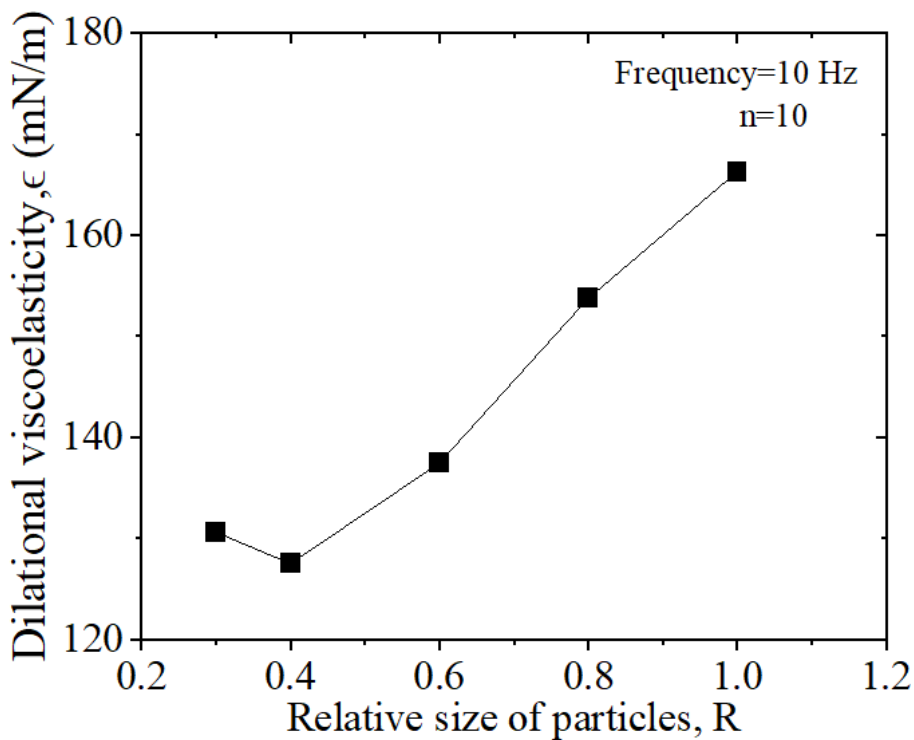


Figure 3.8. The change in dilational viscoelasticity,  $\epsilon$ , as a function of the relative size of particles,  $R$ .  $\epsilon$  increases as the aggregate size increases.

## CHAPTER 4: CONCLUSION AND FUTURE WORK

We have established parameters that manifest the fate of heteroaggregation of lignin-zein nanoparticles in this thesis. pH plays a crucial role in manipulating the charge of particles suspended in an aqueous medium. Measuring zeta potential as a function of pH of each pure component is an effective way in predicting the stability of particles and the likelihood of heteroaggregate formation. Particles express high stability when they possess alike charges. Conversely, heteroaggregates are formed when the particles are oppositely charged. A high relative concentration and relative size of lignin to zein particles gives rise to a core-shell structure that is stable against the formation of aggregates.

Heteroaggregates were able to adsorb at the oil-water interface and reduce IFT. The droplet oscillatory was performed to determine the viscoelastic property of the interfacial film formed because of heteroaggregate adsorption. The results found in this work suggested that large aggregates were able to produce a more stable interfacial film than small aggregates. The interfacial film made of aggregates behaves as a rigid barrier from 0.1-7 Hz and an elastic barrier at higher frequencies.

The frequency-specific response of the interfacial film should be explored more in future work. Due to the limitation of the tensiometer, the highest frequency performed here was 10 Hz. Thus, it is unknown how the film will behave at a frequency higher than 10 Hz. In addition, adsorption of aggregates at low concentration requires further investigation.

Understanding more parameters that impact the property of the interfacial films can imprint a promising application in stabilizing the oil-water interface. Researchers have been creating one dimensional nanofilms through adsorption of nanoparticles onto oil-water interface

(Hu et al., 2012). Further investigation on self-assembly of nanofilm of lignin-zein aggregates at oil-water should be conducted to explore the mechanical property of the film, which may be applied to create novel membranes or an emulsion stabilizer agent.

## REFERENCE

- (1) Azimzada, A., Jreije, I., Hadioui, M., Shaw, P., Farner, J. M., & Wilkinson, K. J. (2021). Quantification and Characterization of Ti-, Ce-, and Ag-Nanoparticles in Global Surface Waters and Precipitation. *Environmental Science and Technology*, 55(14), 9836–9844. <https://doi.org/10.1021/acs.est.1c00488>
- (2) Bayda, S., Adeel, M., Tuccinardi, T., Cordani, M., & Rizzolio, F. (2020). The history of nanoscience and nanotechnology: From chemical-physical applications to nanomedicine. In *Molecules* (Vol. 25, Issue 1). MDPI AG. <https://doi.org/10.3390/molecules25010112>
- (3) Berry, J. D., Neeson, M. J., Dagastine, R. R., Chan, D. Y. C., & Tabor, R. F. (2015). Measurement of surface and interfacial tension using pendant drop tensiometry. In *Journal of Colloid and Interface Science* (Vol. 454, pp. 226–237). Academic Press Inc. <https://doi.org/10.1016/j.jcis.2015.05.012>
- (4) Bharti, B., Meissner, J., & Findenegg, G. H. (2011). Aggregation of silica nanoparticles directed by adsorption of lysozyme. *Langmuir*, 27(16), 9823–9833. <https://doi.org/10.1021/la201898v>
- (5) Bhattacharjee, S. (2016). DLS and zeta potential - What they are and what they are not? In *Journal of Controlled Release* (Vol. 235, pp. 337–351). Elsevier B.V. <https://doi.org/10.1016/j.jconrel.2016.06.017>
- (6) Binks, B. P. (2002). *ELSEVIER SCIENCE DIRECT Particles as surfactants similarities and differences*.
- (7) Edward, J. T. (1970). *Molecular Volumes and the Stokes-Einstein Equation*. <https://pubs.acs.org/sharingguidelines>
- (8) Elmobarak, W. F., & Almomani, F. (2021). Application of Fe<sub>3</sub>O<sub>4</sub> magnetite nanoparticles grafted in silica (SiO<sub>2</sub>) for oil recovery from oil in water emulsions. *Chemosphere*, 265. <https://doi.org/10.1016/j.chemosphere.2020.129054>
- (9) Feng, Y., & Lee, Y. (2016). Surface modification of zein colloidal particles with sodium caseinate to stabilize oil-in-water pickering emulsion. *Food Hydrocolloids*, 56, 292–302. <https://doi.org/10.1016/j.foodhyd.2015.12.030>

- (10) Feng, Y., Liu, X., Huynh, K. A., McCaffery, J. M., Mao, L., Gao, S., & Chen, K. L. (2017). Heteroaggregation of Graphene Oxide with Nanometer- and Micrometer-Sized Hematite Colloids: Influence on Nanohybrid Aggregation and Microparticle Sedimentation. *Environmental Science and Technology*, *51*(12), 6821–6828. <https://doi.org/10.1021/acs.est.7b00132>
- (11) Goldberg, W. I. (1999). Dynamic light scattering. *American Journal of Physics*, *67*(12), 1152–1160. <https://doi.org/10.1119/1.19101>
- (12) Holley, N. P., Lee, J. G., Valsaraj, K. T., & Bharti, B. (2021). Synthesis and characterization of ZEin-based Low Density Porous Absorbent (ZELDA) for oil spill recovery. *Colloids and Surfaces A: Physicochemical and Engineering Aspects*, *614*. <https://doi.org/10.1016/j.colsurfa.2021.126148>
- (13) Hotze, E. M., Phenrat, T., & Lowry, G. v. (2010). Nanoparticle Aggregation: Challenges to Understanding Transport and Reactivity in the Environment. *Journal of Environmental Quality*, *39*(6), 1909–1924. <https://doi.org/10.2134/jeq2009.0462>
- (14) Hu, L., Chen, M., Fang, X., & Wu, L. (2012). Oil–water interfacial self-assembly: A novel strategy for nanofilm and nanodevice fabrication. *Chemical Society Reviews*, *41*(3), 1350–1362. <https://doi.org/10.1039/c1cs15189d>
- (15) Hua, X., Frechette, J., & Bevan, M. A. (2018). Nanoparticle adsorption dynamics at fluid interfaces. *Soft Matter*, *14*(19), 3818–3828. <https://doi.org/10.1039/c8sm00273h>
- (16) Jia, L., Chen, R., Xu, J., Zhang, L., Chen, X., Bi, N., Gou, J., & Zhao, T. (2021). A stick-like intelligent multicolor nano-sensor for the detection of tetracycline: The integration of nano-clay and carbon dots. *Journal of Hazardous Materials*, *413*. <https://doi.org/10.1016/j.jhazmat.2021.125296>
- (17) Jin, P., Wiraja, C., Zhao, J., Zhang, J., Zheng, L., & Xu, C. (2017). Nitric Oxide Nanosensors for Predicting the Development of Osteoarthritis in Rat Model. *ACS Applied Materials and Interfaces*, *9*(30), 25128–25137. <https://doi.org/10.1021/acsami.7b06404>
- (18) Khaliq, N., Rasheed, M. A., Khan, M., Maqbool, M., Ahmad, M., Karim, S., Nisar, A., Schmuki, P., Cho, S. O., & Ali, G. (2021). Voltage-Switchable Biosensor with Gold Nanoparticles on TiO<sub>2</sub>Nanotubes Decorated with CdS Quantum Dots for the Detection of Cholesterol and H<sub>2</sub>O<sub>2</sub>. *ACS Applied Materials and Interfaces*, *13*(3), 3653–3668. <https://doi.org/10.1021/acsami.0c19979>

- (19) Lee, J. G., Larive, L. L., Valsaraj, K. T., & Bharti, B. (2018). Binding of Lignin Nanoparticles at Oil-Water Interfaces: An Ecofriendly Alternative to Oil Spill Recovery. *ACS Applied Materials and Interfaces*, *10*(49), 43282–43289. <https://doi.org/10.1021/acsami.8b17748>
- (20) Lin, J. L., Pan, J. R., & Huang, C. (2013). Enhanced particle destabilization and aggregation by flash-mixing coagulation for drinking water treatment. *Separation and Purification Technology*, *115*, 145–151. <https://doi.org/10.1016/J.SEPPUR.2013.05.013>
- (21) Pothipor, C., Aroonyadet, N., Bamrungsap, S., Jakmunee, J., & Ounnunkad, K. (2021). A highly sensitive electrochemical microRNA-21 biosensor based on intercalating methylene blue signal amplification and a highly dispersed gold nanoparticles/graphene/polypyrrole composite. *Analyst*, *146*(8), 2679–2688. <https://doi.org/10.1039/d1an00116g>
- (22) Ravera, F., Loglio, G., & Kovalchuk, V. I. (2010). Interfacial dilational rheology by oscillating bubble/drop methods. In *Current Opinion in Colloid and Interface Science* (Vol. 15, Issue 4, pp. 217–228). <https://doi.org/10.1016/j.cocis.2010.04.001>
- (23) Ravera, F., Santini, E., Loglio, G., Ferrari, M., & Liggieri, L. (2006). Effect of nanoparticles on the interfacial properties of liquid/liquid and liquid/air surface layers. *Journal of Physical Chemistry B*, *110*(39), 19543–19551. <https://doi.org/10.1021/jp0636468>
- (24) Richter, A. P., Bharti, B., Armstrong, H. B., Brown, J. S., Plemmons, D., Paunov, V. N., Stoyanov, S. D., & Velev, O. D. (2016). Synthesis and characterization of biodegradable lignin nanoparticles with tunable surface properties. *Langmuir*, *32*(25), 6468–6477. <https://doi.org/10.1021/acs.langmuir.6b01088>
- (25) Richter, A. P., Brown, J. S., Bharti, B., Wang, A., Gangwal, S., Houck, K., Cohen Hubal, E. A., Paunov, V. N., Stoyanov, S. D., & Velev, O. D. (2015). An environmentally benign antimicrobial nanoparticle based on a silver-infused lignin core. *Nature Nanotechnology*, *10*(9), 817–823. <https://doi.org/10.1038/nnano.2015.14>
- (26) Smith, B. M., Pike, D. J., Kelly, M. O., & Nason, J. A. (2015). Quantification of Heteroaggregation between Citrate-Stabilized Gold Nanoparticles and Hematite Colloids. *Environmental Science and Technology*, *49*(21), 12789–12797. <https://doi.org/10.1021/acs.est.5b03486>

- (27) Spruijt, E., Bakker, H. E., Kodger, T. E., Sprakel, J., Cohen Stuart, M. A., & van der Gucht, J. (2011). Reversible assembly of oppositely charged hairy colloids in water. *Soft Matter*, 7(18), 8281–8290. <https://doi.org/10.1039/c1sm05881a>
- (28) Trefalt, G., & Borkovec, M. (2014). *Overview of DLVO Theory*. [www.colloid.ch/dlvo](http://www.colloid.ch/dlvo)
- (29) Whitby, C. P., Fornasiero, D., Ralston, J., Liggieri, L., & Ravera, F. (2012). Properties of fatty amine-silica nanoparticle interfacial layers at the hexane-water interface. In *Journal of Physical Chemistry C* (Vol. 116, Issue 4, pp. 3050–3058). <https://doi.org/10.1021/jp210870v>
- (30) Xin, Q. qi, Chen, X., Yuan, R., Yuan, Y. hui, Hui, J. qi, Miao, Y., Cong, W. hong, & Chen, K. ji. (2021). Correlation of Platelet and Coagulation Function with Blood Stasis Syndrome in Coronary Heart Disease: A Systematic Review and Meta-Analysis. *Chinese Journal of Integrative Medicine*. <https://doi.org/10.1007/s11655-021-2871-2>
- (31) Zeppieri, S., Rodríguez, J., & López De Ramos, A. L. (2001). Interfacial tension of alkane + water systems. *Journal of Chemical and Engineering Data*, 46(5), 1086–1088. <https://doi.org/10.1021/je000245r>
- (32) Zhang, Y., Wang, S., Zhou, J., Zhao, R., Benz, G., Tcheimou, S., Meredith, J. C., & Behrens, S. H. (2017). Interfacial Activity of Nonamphiphilic Particles in Fluid-Fluid Interfaces. *Langmuir*, 33(18), 4511–4519. <https://doi.org/10.1021/acs.langmuir.7b00599>
- (33) Zhao, D., Zhang, Q., Zhang, Y., Liu, Y., Pei, Z., Yuan, Z., & Sang, S. (2019). Sandwich-type Surface Stress Biosensor Based on Self-Assembled Gold Nanoparticles in PDMS Film for BSA Detection. *ACS Biomaterials Science and Engineering*, 5(11), 6274–6280. <https://doi.org/10.1021/acsbiomaterials.9b01073>

## **Vita**

Yada Chulakham was born in Rayong, Thailand. She attended North Carolina State University in August 2014 and received the degree of Bachelor of Science in Chemical Engineering in May 2017. In 2019, she entered Louisiana State University and received the degree of Master of Science in Chemical Engineering in May 2022.